Actin Reorganization through Dynamic Interactions with Single-Wall Carbon Nanotubes

Hengameh Shams,[†,‡] Brian D. Holt,[§] Seyed Hanif Mahboobi,[†] Zeinab Jahed,[†] Mohammad F. Islam,[⊥] Kris Noel Dahl,[§,∥] and Mohammad R. K. Mofrad[†,‡,*]

[†]Molecular Cell Biomechanics Laboratory, Departments of Bioengineering and Mechanical Engineering, University of California, Berkeley, California 94720, United States, [‡]Physical Biosciences Division, Lawrence Berkeley National Lab, Berkeley, California 94720, United States , [§]Department of Biomedical Engineering, Carnegie Mellon University, Pittsburgh, Pennsylvania 15213, United States, [⊥]Department of Materials Science and Engineering, Carnegie Mellon University, Pittsburgh, Pennsylvania 15213, United States, and [∥]Department of Chemical Engineering, Carnegie Mellon University, Pittsburgh, Pennsylvania 15213, United States

ABSTRACT Single-wall carbon nanotubes (SWCNTs) have been widely used for biological applications in recent years, and thus, it is critical to understand how these inert nanomaterials influence cell behavior. Recently, it has been observed that cellular phenotypes such as proliferation, force generation and growth change upon SWCNT treatment, and SWCNTs directly affect the organization and redistribution of the actin cytoskeleton. However, the interactions between SWCNTs and actin at the molecular level or how this interaction changes actin structure remain largely unknown. Here, we investigated direct interaction of actin with SWCNT using all-atom molecular dynamics simulations and NIR spectroscopy of actin-dispersed SWCNTs. Actin can stably bind to the SWCNT surfaces *via* hydrophobic interactions but still allows nanotubes to slide and rotate on the actin surface. Our results establish several nanoscale conformational changes for the actin–SWCNT complexes, and we suggest these changes likely induce reorganization of actin filaments observed at larger scales.

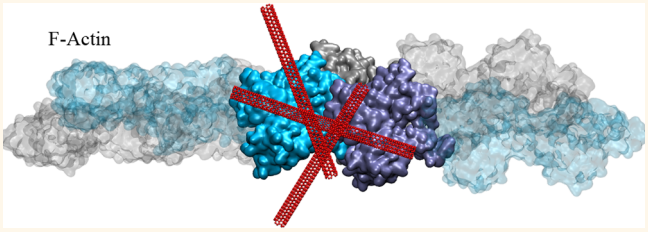

KEYWORDS: actin · single-walled carbon nanotubes · molecular dynamics · cytoskeleton · near-infrared fluorescence spectroscopy

The design and engineering of nanoscale devices for biomedical applications require a more thorough understanding of principles governing physical phenomena at this scale. Due to their extraordinary mechanical, chemical, optical and thermal properties, carbon nanotube (CNT)-based devices have attracted major attention in a variety of applications ranging from scaffolds for neural tissue growth to gene delivery.[1−5] More recently, studies have shown that CNT insertion in various cell types is possible, making them a promising tool for intracellular transport.[6−10] Due to their biocompatibility[11] and unique ability to translocate through the plasma membrane and the nuclear envelope, *via* the nuclear pore complex,[12] without harming cell viability,[6] CNTs have been used for the intracellular and nuclear delivery of various biological cargos such as proteins, peptides DNA, and nucleic acids.[7−10,13−17]

CNTs can be synthesized as single- or multiple-layer tubular structures with a wide range of different properties. Single-wall carbon nanotubes (SWCNTs) are preferred for biomedical applications for reasons such as their high length to diameter aspect ratio, high axial stiffness, inactivity in chemical reactions and negligible fluctuations at body temperature. While several studies have examined the thermal, chemical and mechanical properties of CNTs,[18−21] for biological applications, where the introduction of external agents can disrupt natural functionalities of cells and thus organs, the specific effects of CNTs on the system behavior must be further explored. Moreover, in some cases the strength of CNT interaction might be of interest. For example, site specific drug deliveries require modifications of CNTs by attaching other molecules and/or ions that increase binding affinities for target molecules.[22] Such processes, usually referred to as functionalization, necessitate a detailed understanding of CNT interactions with both target and newly attached molecules.

* Address correspondence to mofrad@berkeley.edu.

Received for review June 6, 2013 and accepted December 18, 2013.

Published online December 18, 2013
10.1021/nn402865e

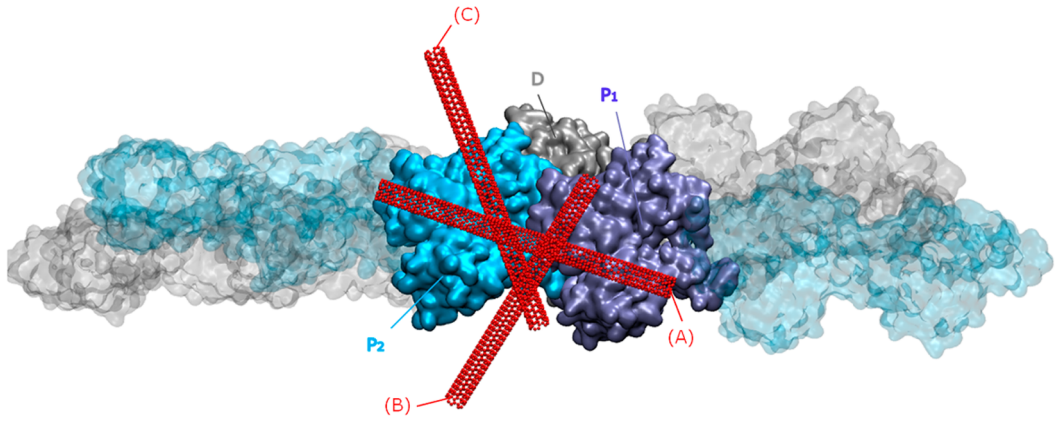

Figure 1. Three distinct initial configurations of SWCNT relative to actin. Orientation (A) of SWCNT was previously found to be favorable[26] for actin binding. Orientations (B) and (C) were generated using docking of SWCNT on the actin trimer in the filamentous order (bold along the actin polymer shown in transparent representation). The two actin monomers proximal to SWCNT are labeled P_1 and P_2, while the third monomer in the neighboring strand that is more distal is labeled D.

Many biological functions of the cell depend highly on filamentous actin (F-actin). For example, cell migration requires continuous reorganization of actin filaments, a dynamic process that is directly influenced by G-actin interaction. Other important cellular processes directly related to F-actin distribution are cell proliferation, differentiation and growth.[23] Any external agent with even a slight affinity for F-actin may affect the intermonomer interaction and thereby influence the force generation machinery within cells that in turn may affect cell adhesion.[24]

Recently, we observed changes in F-actin structures inside the cell upon the uptake of SWCNTs.[24−26] In these previous works, SWCNTs were dispersed using Pluronic F127 (PF127), which is a biocompatible polymer. Our work revealed that the cytoskeletal structure, force generation and proliferation of SWCNT-treated fibroblasts are modified.[26] Actin filaments were shorter and redistributed in the SWCNT-treated cells compared to the control assay. In the same study, the main SWCNT binding sites on actin were investigated. Herein, we present a detailed study on SWCNT interaction with F-actin using both computational and experimental techniques. Specifically, all-atom molecular dynamics simulations were used to characterize the SWCNT−actin interaction, while near-infrared (NIR) fluorescence and Raman spectroscopies confirmed direct interactions between actin and SWCNT (without PF127 polymer) *ex vivo*. In our model, we explored the SWCNT interaction with actin trimer that is an intermediate state before polymerization and contains the primary filamentous interactions.[27] In this study, we investigated the effect of SWCNT on the monomer−monomer interaction, which may potentially influence actin reorganization in the cytoskeleton.

RESULTS

The purpose of this study is to explore the molecular level interactions between actin and SWCNT in order to shed light on the alterations of cell shape and morphology observed in the experimental studies done by Holt *et al.*[24−26] Here, we investigate SWCNT−actin association using both all-atom molecular dynamics (MD) simulations and NIR spectroscopy. For the computational portion of our purpose, we used (5,5)-SWCNT, which has a diameter within the experimental range and a size appropriate for modeling. Three actin monomers arranged in the filamentous order (trimer nucleus) in complex with SWCNT were monitored throughout the simulation. To highlight the effect of SWCNT on the conformation of F-actin and the dynamics of their internal interaction more rigorously, a separate control MD simulation was conducted containing the actin trimer only and was later compared to the SWCNT−actin binding simulations. The control simulation ran for the same time interval and with the same equilibrated structure of the actin trimer as that in the SWCNT binding simulation. (Most of the results are presented in the presence and absence of SWCNT in the same plot and thus referred to as W-CNT and W/O-CNT, respectively, in order to avoid repetition of terms.) In the initial configuration of the trimer, all three monomers were in close contact, two being in the axial direction of the actin filament (referred to as proximal monomers 1 and 2 or 'P_1' and 'P_2' throughout the text). The third monomer is referred to as the distal monomer or 'D' (Figure 1).

Molecular Dynamics Simulations. Distinct orientations of SWCNT relative to actin were generated in order to account for a broad range of binding possibilities between the two inside the cell (Figure 1). First, we used Hex docking server[28] to find the top 10 candidates according to geometry matching. After categorizing similar docked structures, we found two distinct complexes out of which the one with highest geometrical compatibility was selected as a representative for further MD studies. Although results from all three initial configurations showed consistency in some

aspects, each suggest interesting case-specific interactions that are reported separately in the Results section.

In the initial configuration of binding mode A, the SWCNT axis was aligned along the actin filament and positioned proximal to the groove formed between the two actin strands. Previously we found this region to effectively bind to SWCNT.[26] The minimum distance between the nearest carbon atom of the SWCNT structure to actin residues was adjusted to be approximately 0.7 nm. That was within the range of both electrostatic and van der Waals (vdW) forces; however, it allowed water layers to form at the interface in the initial setting prior to any stable binding. It was observed that after less than 3 ns, the SWCNT/actin binding was established. The binding location of SWCNT tends to remain close to the actin groove and further stabilize its position during the simulation confirming our previous results.[26]

Interaction energies—sum of van der Waals and electrostatic terms—were monitored for all three binding modes. The interaction energy of mode A continued to stabilize in the first 10 ns, and it dropped to −140 kcal/mol (Figure 2A). The average energy of binding mode A (−134.23 kcal/mol) was higher than that of mode B (−92.11 kcal/mol) that itself is larger, by approximately the same amount, than mode C energy (−45.93 kcal/mol), implying the stronger SWCNT−actin interaction in mode A (Figure 2B,C). The energies follow the similar trend as the docking analysis.

The solvent accessible surface area (SASA) of SWCNT reached a stable value of 0.5 nm^2 within the first 3 ns (Figure 3). For binding mode B, although the interaction energy was relatively stable, SASA increased in time within the last 20 ns. The SASA plot for mode C fluctuated sharply after 18 ns, showing unstable surface association with actin, which is consistent with the interaction energy. Therefore, SASA alone is not indicative of stable binding per se, and it should be interpreted along with energies. All SASA and energy graphs were averaged over three trials for each binding mode.

Among all the actin residues on the surface involved in SWCNT interactions, 50% were hydrophobic, which is relatively high on an overall hydrophilic surface, including ALA143, VAL29 and TYR336 on P_1, and ALA275, ILE327 and PRO329 on P_2, which were energetically most favorable. SWCNT atoms were assumed to be neutral, thereby, electrostatic interactions were automatically eliminated.

Our results showed that residues capable of forming multiple vdW interactions are crucial for SWCNT association. For instance, residues with aromatic side chains, such as tyrosine, made a number of interactions with carbon rings on the SWCNT surface, which is very similar in appearance to the $\pi\cdots\pi$ bond; however, it should be noted that quantum mechanical effects such

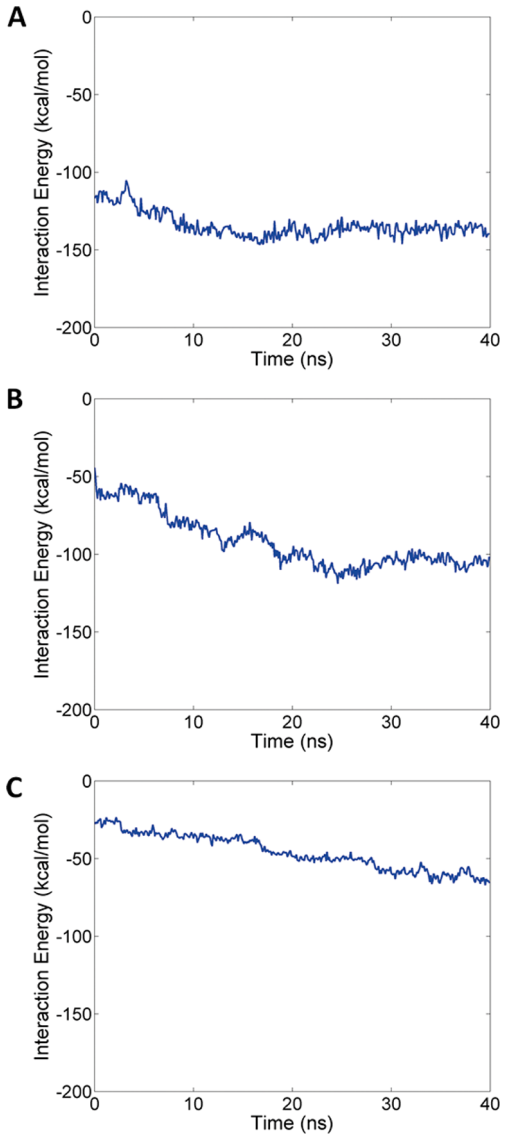

Figure 2. Interaction energy between SWCNT and actin: (A) mode A; (B) mode B; and (C) mode C. All modes show an increase in interaction energy, and the highest and lowest interaction energies were observed in modes A and C, respectively. Mode C was also scored lower than mode B based on docking results. A higher engagement of SWCNT with actin is seen in mode A while the interfacial areas are smaller in all other modes.

as overlap in atomic orbitals are not accounted for in MD simulations. In addition, residues with extended side chains, such as lysine and aspartic acid, also associated strongly to the surface of SWCNT composing a sequence of interactions. Therefore, all polar, charged and nonpolar residues contributed to SWCNT binding.

In all trials, we observed two interesting types of SWCNT motions relative to the actin surface: (1) sliding or translocation along the SWCNT axis and (2) rotational motion around the axis of SWCNT. However, each trial showed some unique characteristics that are worth mentioning individually. Figure 4A shows a long sliding motion for the first trial starting from 5 ns to the

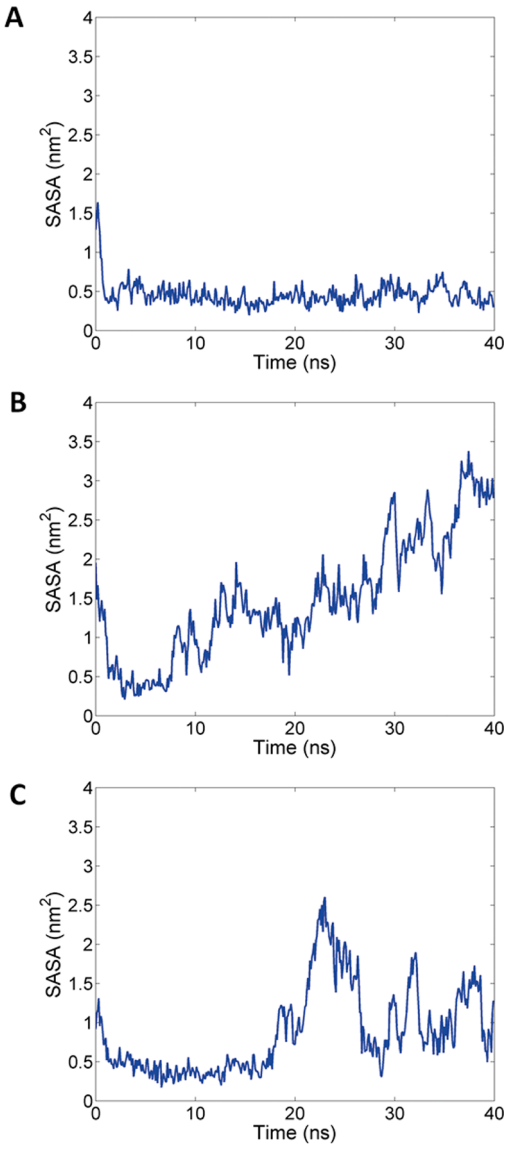

Figure 3. Average solvent accessible surface area (SASA) for SWCNT in three binding modes for (A) mode A, (B) mode B, and (C) mode C. SWCNT in mode A showed the lowest and most stable SASA which is in agreement with its strong stable interaction with actin. The exposed surface of SWCNT decreased to 0.5 nm^2 in less than 2.5 ns indicating a stable interaction with actin throughout the simulation. In contrast to mode A, mode B steadily gains SASA or in other words loses its contact with actin.

end of the 40 ns simulation. However, during the sliding period, there are short intervals, for example between 10 and 15 ns, at which SWCNT is approximately stationary relative to actin. Moreover, the SWCNT sliding motion changed direction at three instances: 18, 20, and 23 ns. One significant rotational motion for the same trial occurred in the first 2.5 ns (Figure 4B). There are two sudden changes in the rotational angle around 10 and 24 ns. Also, the average angle changed from 80° to 60° at 19 ns. In the second trial, the sliding motion changed direction several times, mainly at 5, 25, and 35 ns, while SWCNT was sliding mostly in one direction in the first trial (Figure 4C). However, SWCNT was rotating mostly in one direction throughout the second trial (Figure 4D). The trend of the rotational motion in the third trial is similar to that in the second one (Figure 4F). The sliding motion in the third trial was less significant than that in the other two (Figure 4E).

One trial of both modes B and C (Figures S1A, S1E, S2A and S2C) showed a long directional motion of SWCNT along its axis (~3 nm), while no significant sliding occurred in the other two trials of these modes. However, the rotational motion was notably increased in modes B and C, which is likely to be due to reduced association of SWCNT to actin compared to A.

All carbon atoms, except those at the edges of SWCNT, identically form equi-energy interactions with a certain type of atom. Therefore, although actin residues in the SWCNT/actin interface remained fixed, SWCNT slid along the actin surface, while simultaneously rotating around its own axis. The energy of interaction between P_1 and P_2 shows more stability compared to the control simulation. Despite the relative motion of SWCNT and actin, SASA did not change after the first 8 ns implying that rotation and sliding did not involve any local dissociation of residues (Figure 3).

Figure 5 shows the pairwise interactions within the actin trimer for all binding modes. In the control simulation, the interaction energies of P_1-P_2 and P_2-D slightly increased throughout the simulation, while the distal monomer interaction with P_1 was negligible at all times. The slight repulsion within the actin trimer is most likely an artifact of not having the rest of the actin filament in the model (Figure 5A). Interestingly, the presence of SWCNT stabilized P_1-P_2 and P_2-D interaction regardless of the binding mode (Figure 5B,C). However, P_1-D interaction was enhanced upon SWCNT binding in mode C (Figure 5D).

Both hydrogen bonding and hydrophobic interactions contributed to stabilizing the interface, *e.g.*, ALA727 and GLU194 of P_1 were in contact with ILE368 and ASN110 of D. The fluctuations in radius of gyration (Rg) of none of actin monomers within the trimer in any of the binding modes showed significant variations upon SWCNT binding implying that the overall conformation of F-actin was maintained (Figure S3). The root-mean-square fluctuation of SWCNT was maximized in the middle and both ends, which is in agreement with the previous studies (Figure S4).

SWCNTs–Actin Dispersions. Since our modeling results demonstrated that there is an energetically favorable interaction directly between SWCNTs and F-actin, we experimentally examined the capability of G-actin monomers and polymerized F-actin oligomers to form stable suspensions of individually dispersed nanotubes (see Methods). Note, when nanotubes are added to water, vdW interactions cause them to aggregate and bundle. However, adhering surfactants and macromolecules allow

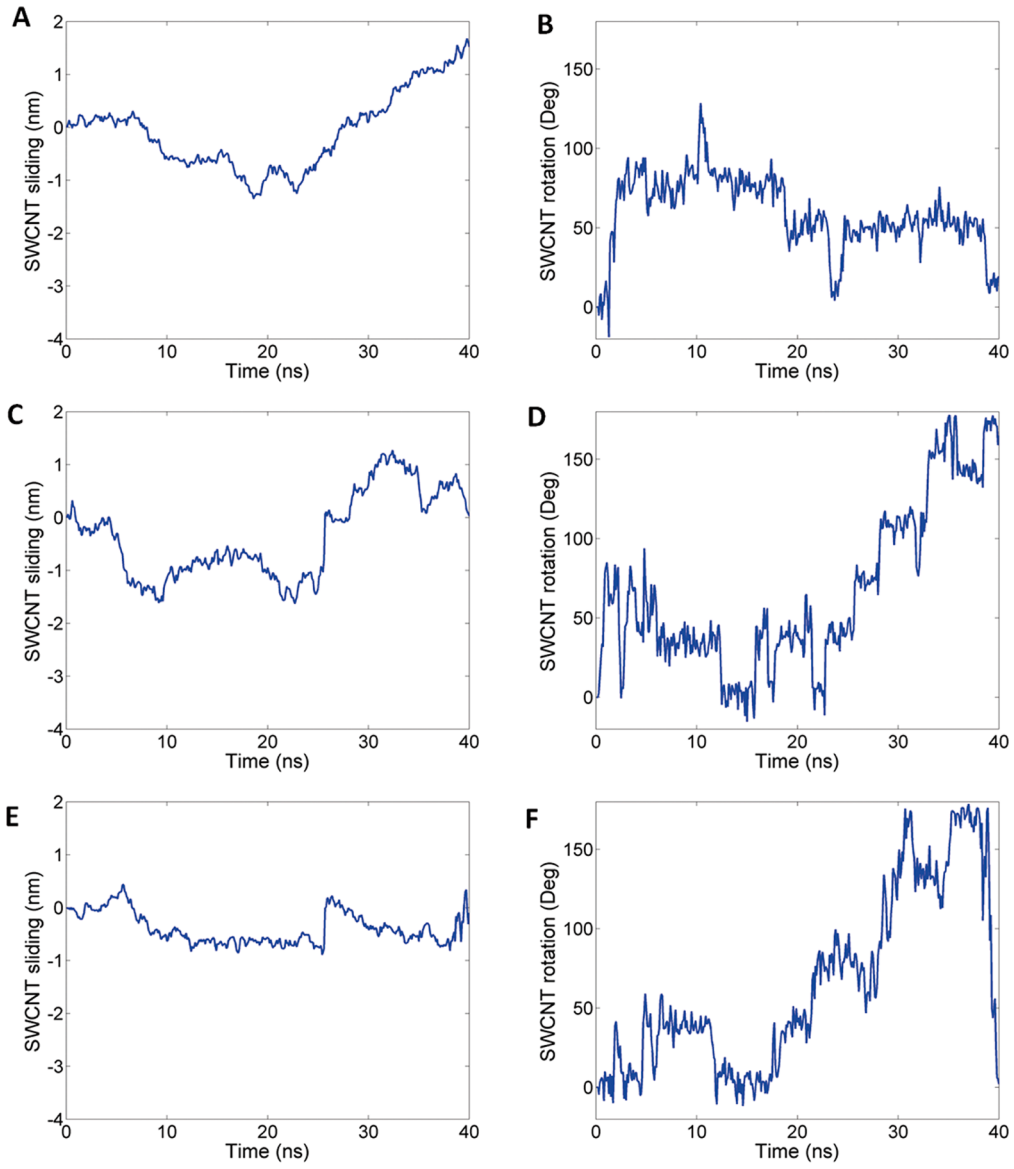

Figure 4. SWCNT sliding and rotation for mode A: (A) Sliding in trial 1; (B) rotation in trial 1; (C) sliding in trial 2; (D) rotation in trial 2; (E) sliding in trial 3; and (F) rotation in trial 3. SWCNT shows different kinematic behavior in each trial which can be attributed to the highly dynamic nature of its interaction with actin. While in trial 1 SWCNT continues to travel in a certain direction starting from the middle of simulation time, in other trials it returns to its original position. On the other hand, SWCNT rotation is lowest in trial 1 in comparison to the other trials. Rotation shows stepwise changes while sliding motion is smoother. Sliding and rotational motions do not appear to be coupled.

SWCNTs to be individually dispersed, a widely used approach to create stable nanotube suspensions. The individualization of nanotubes and the stability of the resultant suspensions qualitatively suggest the interaction strength between the macromolecules and nanotubes. We characterized the SWCNT dispersions by F-actin and G-actin with complementary techniques to determine yield (by UV–vis–NIR absorbance spectroscopy), SWCNT defects (by Raman spectroscopy) and dispersion quality (by NIR fluorescence spectroscopy).

UV–vis–NIR absorbance spectroscopy of dispersed SWCNTs showed numerous peaks (Figure 6A), which indicate that the nanotubes are dispersed in water by both F-actin and G-actin.[29] The yield from G- and F-actin (Figure 6B), determined using a known absorbance coefficient at 930 nm,[25,30−33] is similar not only to the yield from other protein dispersions[30,31] but also to the yield of deoxycholate (DOC)-dispersed SWCNTs: a surfactant that has shown excellent dispersion capability of SWCNTs.[34]

We used Raman spectroscopy to further verify the yield and to quantify the quality of the SWCNTs after the dispersion process (Figure 6C). The intensity of the disorder-band (at ∼1300 cm^{-1}), which represents the number of defects in the SWCNT sp^2 structure, was ∼10% compared to the intensity of the G-band (∼1590 cm^{-1}), which represents the total amount of nanotubes in the suspension.[35] Therefore, we do not

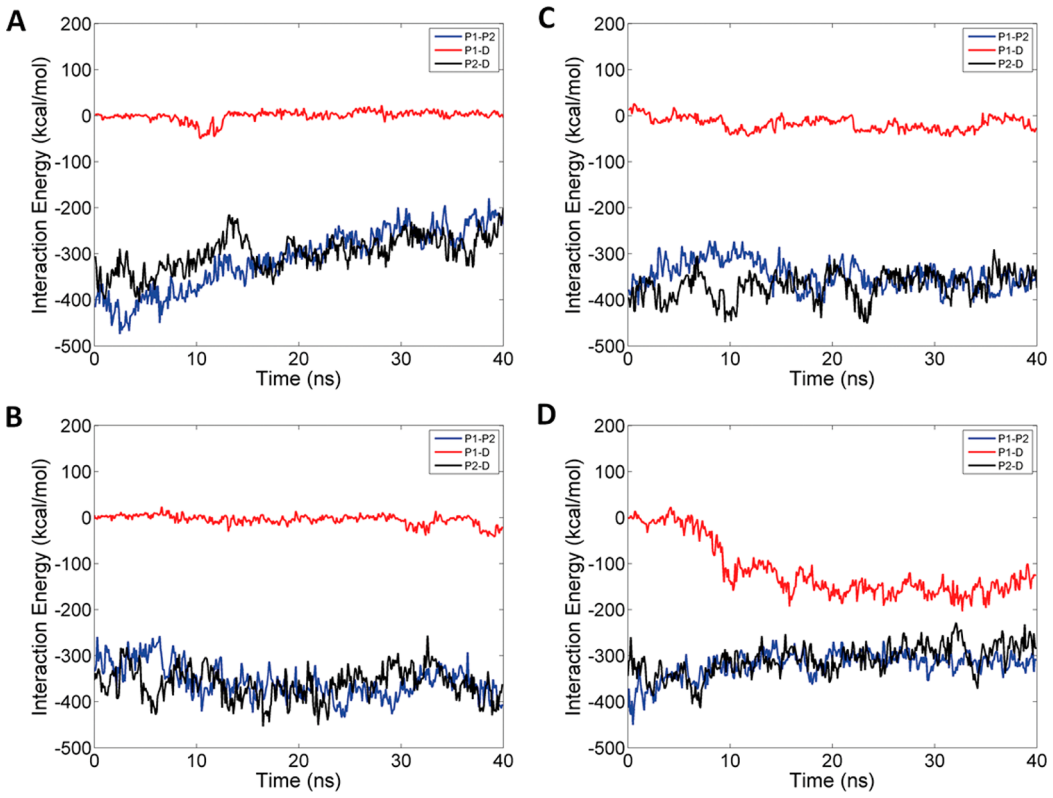

Figure 5. The average pairwise interactions within the trimer. (A) The interaction energies of all possible pairs of actin monomers (see the legend) in the absence of SWCNT. The P_1-P_2 and P_2-D energies are increasing in time although they are relatively stable compared to P_1-D interaction, which is negligible. The interaction energies of all possible pairs of actin monomers in the presence of SWCNT are shown for different binding modes: (B) mode A, (C) mode B, and (D) mode C. In modes A and B the P_1-P_2 and P_2-D interaction energies are stabilized upon SWCNT association, while the third monomer (P_1-D) interaction remained the same. In contrast, the P_1-D interaction gets stronger in mode C. All pairwise energies are averaged over three trials.

think that the dispersion process with F-actin and G-actin introduced defects into the nanotubes.

NIR fluorescence spectroscopy is particularly sensitive to the dispersion quality (*i.e.*, whether nanotubes are individually dispersed or in small bundles).[29,36] NIR fluorescence heatmaps demonstrate that both F-actin (Figure 6D) and G-actin (Figure 6E) were able to individually disperse SWCNTs. However, their fluorescence intensities (insets of Figure 6D,E) are only ~5% of the fluorescence intensity obtained for DOC dispersed SWCNTs (inset of Figure 6F) and ~20% of the fluorescence intensities obtained for other protein dispersed SWCNTs.[31] We suspect that while actin structures can interact with SWCNTs, as demonstrated by our modeling results and as observed experimentally both in cells and *ex vivo*,[25,26] actin likely also generates small bundles of SWCNTs. As a result, actin can provide a high yield of nanotube dispersion (at a similar yield to SWCNTs–DOC) due to small bundles which allow SWCNTs to remain dispersed but are nonfluorescing, resulting in relatively weak fluorescence intensity.

DISCUSSION

It has recently been observed that the cytoskeletal structure of cell is highly influenced by SWCNT insertion at concentration levels more than 30 μg/mL using confocal microscopy.[25,26] In treated cells, actin filaments are observed at the apical surface and are shortened and branched, and stress fiber formation is disturbed. Interestingly, imaging F-actin (with fluorescently labeled phalloidin) *versus* G-actin (with fluorescently labeled DNase) shows stronger interaction of SWCNTs with F-actin, despite the entropic advantages of the monomeric G-actin. Furthermore, the traction forces on the substrate are reduced in SWCNT-treated cells. However, these previous studies used a surfactant polymer (PF127) to disperse SWCNTs in water. In cells, it is unclear if the PF127 is lost due to numerous membrane interactions and/or displacement by proteins. Here, we investigate the direct interaction between actin and SWCNT (without PF127) using both all-atom MD and NIR fluorescence spectroscopy in order to investigate the correlation between the observations mentioned above and the SWCNT–actin interaction with high precision. The experimental evidence that actin can directly disperse SWCNTs in water justifies our initial simulation conditions that the SWCNT and actin filament can stably and directly interact.

We observed a stable binding interaction forming between SWCNT and actin, particularly in mode A and somewhat in mode B. Interfacial residues of actin in contact with SWCNT are mostly hydrophobic since

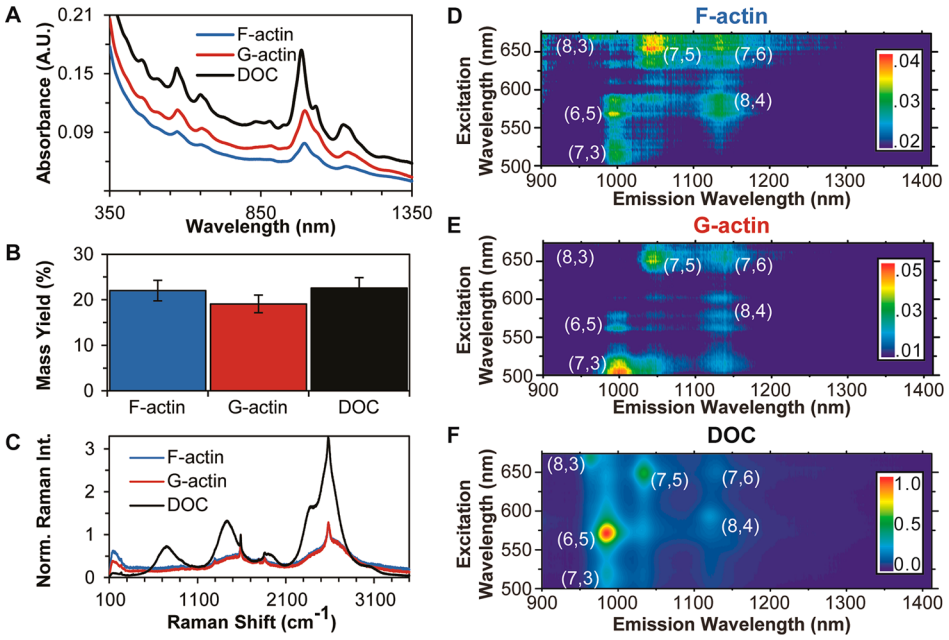

Figure 6. SWCNTs–actin dispersions characterization. (A) UV–vis–NIR absorbance spectroscopy of SWCNTs–actin dispersions. The peaks arise from the van Hove singularities of the density of states and qualitatively indicate dispersion quality. (B) Using a known absorbance coefficient at 930 nm[33] and known initial masses and final volumes, the proportion of SWCNTs remaining in the supernatant after centrifugation was determined and indicated relatively efficient dispersion of SWCNTs, especially for proteins.[31] (C) Raman spectroscopy confirmed the presence of SWCNTs (G-band at ~1591 cm^{-1} and radial breathing modes (150–300 cm^{-1})).[35] For comparison, the data is normalized to each sample's G-band. Note that the large, board peak at ~2200–2900 cm^{-1} primarily arises from real space SWCNT fluorescence at ~950–1016 nm that is unfiltered in our system. (D–F) NIR fluorescence spectroscopy heat maps of SWCNT fluorescence. Chiralities are indicated on the heat maps for visual aid. The color scale bar inset indicates the dynamic range of the intensity range scaling (normalized to DOC).

SWCNT was treated as an electrically neutral and nonpolar molecule. Although the density of hydrophobic residues is not high on the actin surface, we observed that 50% of all interactions in mode A, which showed the largest interface of actin with SWCNT, were hydrophobic demonstrating that SWCNT preferred a local hydrophobic region as its binding site. Moreover, we observed that all residues with planar and extended side chains were able to form multiple vdW contacts with carbon atoms of SWCNT. As a result, all polar, charged and nonpolar residues can contribute to stabilizing SWCNT binding.

An interesting phenomenon observed in the simulation was the 'surface rubbing' of SWCNT on actin in two independent directions: (1) sliding along and (2) rotating about its own axis (see Figure 4). Although we quantified the average behavior of all binding modes, the unique characteristics of sliding and rotational motions in each mode, such as directionality and duration, were also independently studied. The results from these studies indicated that the dynamics of sliding and rotational motion was mainly due to thermal fluctuation of residues on actin surface. Interestingly, the rotational motion showed a stepwise behavior; however, the frequency could not be specified since it is most likely associated with the thermal motion of actin residues, which is random in nature. Conversely, sliding motion was continuous and in some cases even directional. We could not find any specific strong coupling between sliding and rotation; however, there were instances in which weak correlations were observed. In these observations, rotation and sliding occurred subsequently where rotation preceded sliding (Figure 4). One possible reason for 'surface rubbing' could be the hydrophobic forces pushing SWCNT atoms toward the actin surface and thus hydrophobicity of the region around the bound interface may determine the direction of motion. From our results we infer that, statistically, actin atom is likely to associate with all SWCNT carbons with equal interaction energy; thus, the entropic forces promote maximizing sampling of the phase space. Therefore, the combined sliding and rotational motions could be interpreted as the spatial sampling of the SWCNT surface. Potential controllability of the sliding motion may have interesting applications such as cytoskeletal remodeling and drug release.

Therefore, both entropic and hydrophobic forces are responsible for actin redistribution inside the cell; however, our results showed that actin–SWCNT interaction is also energetically favorable. Moreover, direct dispersion of SWCNTs by F-actin observed by NIR fluorescence spectroscopy was in agreement with the MD simulations. Since actin filaments tend to associate with SWCNT, the intramonomer interaction may be modified in longer time-scales that may in turn

affect the intrinsic properties of actin filaments such as mechanical stability. We also observed a reduced NIR fluorescence of actin-dispersed SWCNTs compared with the yield by UV−vis−NIR absorbance and Raman spectroscopy experiments. This suggests that SWCNTs are dispersed as small bundles, perhaps suggesting the energetically favorable state of nanotubes with small bundles of actin filaments. Sliding motion of SWCNT may contribute to changing the dynamics of cytoskeletal redistribution and bundling capability of F-actin as well as force bearing properties such as persistence length and bending stiffness. In addition, SWCNTs change the affinity of F-actins for each other.

The pairwise interaction between proximal actin monomers (P_1-P_2) upon SWCNT association is enhanced since the attraction of actin toward SWCNT cancels out the slight repulsion between the monomers (Figure 2A). Interestingly, P_1-D interaction was notably increased from negligible values to −150 kcal/mol in mode C. Therefore, intermonomer interactions are affected upon SWCNT binding. One interesting observation was the detachment of the D monomer in one of the mode C trials due to the twist of SWCNT normal to its own axis (Figure S5).

Actin bundling requires cross-linking of actin filaments *via* certain molecules such as α-actinin and filamin.[37−39] The association of actin filaments with SWCNT may hinder actin interaction with α-actinin since its binding site overlaps with mode B, which is located between P_1 and P_2.

Interaction of a single G-actin with SWCNT is energetically less favorable than two actin monomers together. Therefore, it is expected that filament formation precedes SWCNT association. This is indeed consistent with experimental observations of the distribution of fluorescently tagged G-actin and F-actin in normal and SWCNT-treated cells.[26] It can be concluded that SWCNT affinity is a collective effect of actin monomers in the filamentous arrangement.

The RMSF plot of SWCNT shows that fluctuations of carbon atoms in SWCNT were higher in the midpoint and both ends, showing that the most stationary contact area was observed at approximately one-quarter of length from both edges (see Figure S4). The RMSF plot of SWCNT remains unchanged upon actin binding independent of the binding mode indicating that local fluctuations of the SWCNT atoms are not affected by the global motions on actin such as sliding and rotation.

It is noteworthy that the SWCNTs attached to cytoskeletal actins are subject to acto-myosin force generation machinery; especially those closer to the cell edge experience forces in the order of piconewtons. Therefore, it is expected that force transmission machinery would be affected upon SWCNT association prohibiting natural protrusions.

CONCLUSIONS

In summary, our results revealed the dynamics of direct actin−SWCNT interaction in three distinct binding modes. Intermonomer interactions of actin are dependent on the SWCNT binding mode and may be increased or decreased in strength. Therefore, cytoskeletal reorganization is mainly due to the modified pairwise interactions in actin upon SWCNT uptake.

MATERIALS AND METHODS

Docking. Hex interactive docking software was used to generate the initial configurations of the SWCNT−actin complex.[28] Geometric compatibility was taken into account in obtaining the optimized bound structures. The top 10 docking structures were classified into two different classes, from each of which one representative was selected (Figure 1).

Molecular Dynamics Simulations. All molecular dynamics simulations were carried out using NAMD 2.9 molecular dynamics software package[40] and CHARMM27 force field.[41] Periodic boundary conditions were applied in all three directions. The entire system was then minimized for 5000 steps, which was followed by a 1 ns equilibration in constant pressure. The equilibrated structure was then used for studying the binding interaction between SWCNT and actin in a 40 ns-simulation, which ran with 1 fs time-step. Particle mesh Ewald (PME) was applied to model the electrostatic interactions, and the SWITCH algorithm, with cutoff distance of 1.2 nm, was used for calculating van der Waals (vdW) forces. The NPT ensemble was used for the production run to sample our system where pressure and temperature remained constant at 1 bar and 310 K using Langevin's piston and the Nose-Hoover thermostat,[42] respectively. All system preparation, visualization and postprocessing analyses were performed using Visual Molecular Dynamics (VMD) software.[43]

The structure of actin trimer positioned in the filamentous arrangement was obtained from the Protein Data Bank (PDB: 3LUE). This structure was minimized and equilibrated in a water box prior to final simulations in order to remove all bad contacts. SWCNT geometry was generated with both (*n*,*m*) indices set to 5. The length and diameter of SWCNT were chosen to be 11 and 0.67 nm, respectively. Three sets of distinct initial configurations found from docking calculations where SWCNT structure was placed approximate to the equilibrate actin groove region where the closest atoms were more than 0.7 nm away. The explicit water molecules were included to solvate the SWCNT−actin complex (water model: TIP3P). In addition to neutralizing the system, 0.15 mM of KCl ions were added to the simulation box in order to resemble ionic concentrations in cell. The number of atoms for the SWCNT−actin configurations was approximately 300 000.

Experimental Methods. *Preparation of G-actin.* G-actin was prepared using the Actin Filament Biochem Kit (Cytoskeleton, Inc.; Denver, CO, USA) according to manufacturer's recommendations. Briefly, muscle actin (250 μg) was resuspended at 4 °C to 0.4 mg/mL in "General Actin Buffer" plus 0.2 mM ATP. The mixture was left on ice for 3.5 h to completely disassemble small oligomers; then it was centrifuged at 4 °C at 14 000*g* for 15 min. The supernatant was immediately aspirated, diluted in ultrapure water at 4 °C to a final volume of 2 mL (for SWCNT dispersion), and immediately added to SWCNTs for dispersion as described below.

Preparation of F-actin. F-actin oligomers were prepared using the Actin Filament Biochem Kit (Cytoskeleton, Inc.; Denver, CO, USA) according to manufacturer's recommendations. Briefly, muscle actin (250 μg) was resuspended to 1.25 mg/mL in "General Actin Buffer" plus 0.2 mM ATP. The mixture was left on

ice for 50 min to disassemble filaments that formed during freeze/thaw. Concentrated "Actin Polymerization Buffer" was added at 1:10 (v/v,) and the mixture was incubated for 45 min at room temperature. These conditions yield filaments ~0.2 to 3 μm long. The filaments were diluted in ultrapure water to a final volume of 2 mL (for SWCNT dispersion) and immediately added to SWCNTs for dispersion as described below.

SWCNT Dispersion. CoMoCAT single-wall carbon nanotubes (SWCNTs) highly enriched (>~40%) in (6,5) chirality with an aggregate, average diameter of ~0.78 nm and a median SWCNT length of ~1.5 μm (SWeNT SG65; SouthWest NanoTechnologies, Inc.; Norman, OK, USA) were dispersed using G-actin or F-actin oligomers at 1:10 (w/w). Actin mixtures were added to SWCNT powder, and the final sample dilution was 1.3×10^{-3} wt % SWCNTs for sonication. Samples were probe-tip sonicated in a 3 mL glass vial for 2 h at 6 W; then they were centrifuged at 21 000*g* for 7 min. Supernatants were aspirated and characterized *via* optical methods as described below.

SWCNT s–Actin Dispersion Characterization. UV–Vis–NIR Absorbance Spectroscopy: Samples were subjected to ultraviolet–visible–near-infrared (UV–vis–NIR) absorbance spectroscopy (Varian Cary 5000 UV–vis–NIR spectrophotometer). A known absorbance coefficient of 2.6 (abs mL)/(mg mm) at 930 nm[33] was used to calculate final SWCNT concentration. The peaks of absorbance arise from the chirality-specific van Hove singularities of the density of states and qualitatively indicate dispersion quality.

Raman Spectroscopy: Raman spectroscopy (inVia confocal Raman microscope with a 785 nm laser; Renishaw, Inc.) confirmed the presence of SWCNTs: strong G-band at ~1591 cm^{-1} indicating an sp^2 hybridized structure and radial breathing modes (RBMs) at ~150–300 cm^{-1} indicating tube structures with ~1 nm diameters.[35] The presence of individual SWCNTs was confirmed by the presence of RBMs < 250 cm^{-1}, and a generally pristine SWCNT structure (*i.e.,* minimal defects) was confirmed by a small disorder-band (D-band at ~1300 cm^{-1}) to G-band ratio.[35]

NIR Fluorescence Spectroscopy: SWCNT dispersion quality was further analyzed by NIR fluorescence spectroscopy (Nanolog Spectrofluorometer with a liquid-nitrogen-cooled Symphony InGaAs–1700 detector; Horiba Jobin Yvon). The samples were diluted to <0.1 abs cm^{-1} in the NIR and were interrogated with excitation and emission slit widths of 10 nm and an integration time per excitation wavelength of 120 s. The excitation grating was blazed at 500 nm (1200 grooves/mm), and the emission grating was blazed at 1200 nm (150 grooves/mm). Fluorescence heatmaps represent corrected fluorescence intensity normalized by corrected excitation intensity. Nanosizer software was used to identify and mathematically fit each chirality's excitation/emission maxima using a Voigt 2D model.

Conflict of Interest: The authors declare no competing financial interest.

Acknowledgment. This work was supported by the National Science Foundation (grant CBET-0829205 and CAREER Award CBET-0955291 to M.R.K.M. and grants CBET-0708418 and DMR-0619424 to K.N.D. and M.F.I. as well as grant DMR-0645596 to M.F.I.) and the DoD, Air Force Office of Scientific Research, National Defense Science and Engineering Graduate (NDSEG) Fellowship, 32 CFR 168a (B.D.H.). In addition, this research used resources of the National Energy Research Scientific Computing Center, which is supported by the Office of Science of the U.S. Department of Energy under Contract No. DE-AC02-05CH11231.

Supporting Information Available: Several figures are included to best indicate SWCNT–actin binding interaction and associated conformational changes in both. This material is available free of charge *via* the Internet at http://pubs.acs.org.

REFERENCES AND NOTES

1. Yang, W.; Thordarson, P.; Gooding, J. J.; Ringer, S. P.; Braet, F. Carbon Nanotubes for Biological and Biomedical Applications. *Nanotechnology* **2007**, *18*, 412001.
2. Bianco, A.; Kostarelos, K.; Partidos, C. D.; Prato, M. Biomedical Applications of Functionalised Carbon Nanotubes. *Chem. Commun. (Cambridge, U.K.)* **2005**, 571–577.
3. Singh, R.; Pantarotto, D.; McCarthy, D.; Chaloin, O.; Hoebeke, J.; Partidos, C. D.; Briand, J.-P.; Prato, M.; Bianco, A.; Kostarelos, K. Binding and Condensation of Plasmid DNA onto Functionalized Carbon Nanotubes: Toward the Construction of Nanotube-Based Gene Delivery Vectors. *J. Am. Chem. Soc.* **2005**, *127*, 4388–4396.
4. Harrison, B. S.; Atala, A. Carbon Nanotube Applications for Tissue Engineering. *Biomaterials* **2007**, *28*, 344–353.
5. Pantarotto, D.; Singh, R.; McCarthy, D.; Erhardt, M.; Briand, J.-P.; Prato, M.; Kostarelos, K.; Bianco, A. Functionalized Carbon Nanotubes for Plasmid DNA Gene Delivery. *Angew. Chem., Int. Ed.* **2004**, *43*, 5242–5246.
6. Kostarelos, K.; Lacerda, L.; Pastorin, G.; Wu, W.; Wieckowski, S.; Luangsivilay, J.; Godefroy, S.; Pantarotto, D.; Briand, J.-P.; Muller, S.; *et al.* Cellular Uptake of Functionalized Carbon Nanotubes Is Independent of Functional Group and Cell Type. *Nat. Nanotechnol.* **2007**, *2*, 108–113.
7. Pantarotto, D.; Briand, J.-P.; Prato, M.; Bianco, A. Translocation of Bioactive Peptides across Cell Membranes by Carbon Nanotubes. *Chem. Commun. (Cambridge, U.K.)* **2004**, 16–17.
8. Shi Kam, N. W.; Jessop, T. C.; Wender, P. A.; Dai, H. Nanotube Molecular Transporters: Internalization of Carbon Nanotube-Protein Conjugates into Mammalian Cells. *J. Am. Chem. Soc.* **2004**, *126*, 6850–6851.
9. Kam, N. W. S.; Liu, Z.; Dai, H. Carbon Nanotubes as Intracellular Transporters for Proteins and DNA: An Investigation of the Uptake Mechanism and Pathway. *Angew. Chem., Int. Ed.* **2006**, *45*, 577–581.
10. Heller, D. A.; Baik, S.; Eurell, T. E.; Strano, M. S. Single-Walled Carbon Nanotube Spectroscopy in Live Cells: Towards Long-Term Labels and Optical Sensors. *Adv. Mater.* **2005**, *17*, 2793–2799.
11. Smart, S. K.; Cassady, A. I.; Lu, G. Q.; Martin, D. J. The Biocompatibility of Carbon Nanotubes. *Carbon* **2006**, *44*, 1034–1047.
12. Jamali, T.; Jamali, Y.; Mehrbod, M.; Mofrad, M.R.K. Nuclear Pore Complex: Biochemistry and Biophysics of Nucleocytoplasmic Transport in Health and Disease. *Int. Rev. Cell Mol. Biol.* **2011**, *287*, 233–286.
13. Kam, N. W. S.; Dai, H. Carbon Nanotubes as Intracellular Protein Transporters: Generality and Biological Functionality. *J. Am. Chem. Soc.* **2005**, *127*, 6021–6026.
14. Cherukuri, P.; Bachilo, S. M.; Litovsky, S. H.; Weisman, R. B. Near-Infrared Fluorescence Microscopy of Single-Walled Carbon Nanotubes in Phagocytic Cells. *J. Am. Chem. Soc.* **2004**, *126*, 15638–15639.
15. Lu, Q.; Moore, J. M.; Huang, G.; Mount, A. S.; Rao, A. M.; Larcom, L. L.; Ke, P. C. RNA Polymer Translocation with Single-Walled Carbon Nanotubes. *Nano Lett.* **2004**, *4*, 2473–2477.
16. Bianco, A.; Hoebeke, J.; Godefroy, S.; Chaloin, O.; Pantarotto, D.; Briand, J.-P.; Muller, S.; Prato, M.; Partidos, C. D. Cationic Carbon Nanotubes Bind to CpG Oligodeoxynucleotides and Enhance Their Immunostimulatory Properties. *J. Am. Chem. Soc.* **2005**, *127*, 58–59.
17. Lacerda, L.; Raffa, S.; Prato, M.; Bianco, A.; Kostarelos, K. Cell-Penetrating CNTs For Delivery of Therapeutics. *Nano Today* **2007**, *2*, 38–43.
18. Dresselhaus, B. M. S.; Dresselhaus, G.; Charlier, J. C. Electronic, Thermal and Mechanical Properties of Carbon Nanotubes. *Philos. Trans. R. Soc., A* **2004**, 2065–2098.
19. Odom, T. W.; Huang, J. Atomic Structure and Electronic Properties of Single-Walled Carbon Nanotubes. *Nature* **1998**, *391*, 1997–1999.
20. Treacy, M. M. J.; Ebbesen, T. W.; Gibson, J. M. Exceptionally High Young's Modulus Observed for Individual Carbon Nanotubes. *Nature* **1996**, *381*, 678–680.
21. Benedict, L. X.; Louie, S. G.; Cohen, M. L. Heat Capacity of Carbon Nanotubes. *Solid State Commun.* **1996**, *100*, 177–180.
22. Zhang, W.; Zhang, Z.; Zhang, Y. The Application of Carbon Nanotubes in Target Drug Delivery Systems for Cancer Therapies. *Nanoscale Res. Lett.* **2011**, *6*, 555.

23. Mofrad, M. R. K.; Kamm, R. D, Eds. *Cytoskeletal Mechanics: Models and Measurements in Cell Mechanics*; Cambridge University Press: Cambridge, U.K., 2011.
24. Yaron, P. N.; Holt, B. D.; Short, P. A.; Lösche, M.; Islam, M. F.; Dahl, K. N. Single Wall Carbon Nanotubes Enter Cells by Endocytosis and Not Membrane Penetration. *J. Nanobiotechnol.* **2011**, *9*, 45.
25. Holt, B. D.; Short, P. A.; Rape, A. D.; Wang, Y.; Islam, M. F.; Dahl, K. N. Carbon Nanotubes Reorganize Actin Structures in Cells and *ex Vivo*. *ACS Nano* **2010**, *4*, 4872–4878.
26. Holt, B. D.; Shams, H.; Horst, T. A.; Basu, S.; Rape, A. D.; Wang, Y.-L.; Rohde, G. K.; Mofrad, M. R. K.; Islam, M. F.; Dahl, K. N. Altered Cell Mechanics from the Inside: Dispersed Single Wall Carbon Nanotubes Integrate with and Restructure Actin. *J. Funct. Biomater.* **2012**, *3*, 398–417.
27. Tuszynski, J. A.; Brown, J. A.; Sept, D. Models of the Collective Behavior of Proteins in Cells: Tubulin, Actin and Motor Proteins. *J. Biol. Phys.* **2003**, *29*, 401–428.
28. Macindoe, G.; Mavridis, L.; Venkatraman, V.; Devignes, M.-D.; Ritchie, D. W. HexServer: An FFT-Based Protein Docking Server Powered by Graphics Processors. *Nucleic Acids Res.* **2010**, *38*, W445–9.
29. O'Connell, M. J.; Bachilo, S. M.; Huffman, C. B.; Moore, V. C.; Strano, M. S.; Haroz, E. H.; Rialon, K. L.; Boul, P. J.; Noon, W. H.; Kittrell, C.; *et al.* Band Gap Fluorescence from Individual Single-Walled Carbon Nanotubes. *Science* **2002**, *297*, 593–596.
30. Holt, B. D.; Dahl, K. N.; Islam, M. F. Quantification of Uptake and Localization of Bovine Serum Albumin-Stabilized Single-Wall Carbon Nanotubes in Different Human Cell Types. *Small* **2011**, *7*, 2348–2355.
31. Holt, B. D.; McCorry, M. C.; Boyer, P. D.; Dahl, K. N.; Islam, M. F. Not All Protein-Mediated Single-Wall Carbon Nanotube Dispersions Are Equally Bioactive. *Nanoscale* **2012**, *4*, 7425–7434.
32. Holt, B. D.; Dahl, K. N.; Islam, M. F.; Al, H. E. T. Cells Take Up and Recover from Protein-Stabilized Single-Wall Carbon Nanotubes with Two Distinct Rates. *ACS Nano* **2012**, *6*, 3481–3490.
33. Fagan, J. A.; Becker, M. L.; Chun, J.; Hobbie, E. K. Length Fractionation of Carbon Nanotubes Using Centrifugation. *Adv. Mater.* **2008**, *20*, 1609–1613.
34. Wenseleers, W.; Vlasov, I. I.; Goovaerts, E.; Obraztsova, E. D.; Lobach, A. S.; Bouwen, A. Efficient Isolation and Solubilization of Pristine Single-Walled Nanotubes in Bile Salt Micelles. *Adv. Funct. Mater.* **2004**, *14*, 1105–1112.
35. Dresselhaus, M. S.; Dresselhaus, G.; Saito, R.; Jorio, A. Raman Spectroscopy of Carbon Nanotubes. *Phys. Rep.* **2005**, *409*, 47–99.
36. Bachilo, S. M.; Strano, M. S.; Kittrell, C.; Hauge, R. H.; Smalley, R. E.; Weisman, R. B. Structure-Assigned Optical Spectra of Single-Walled Carbon Nanotubes. *Science* **2002**, *298*, 2361–2366.
37. Kolahi, K. S.; Mofrad, M. R. K. Molecular Mechanics of Filamin's Rod Domain. *Biophys. J.* **2008**, *94*, 1075–1083.
38. Golji, J.; Collins, R.; Mofrad, M. R. K. Molecular Mechanics of the α-actinin Rod Domain: Bending, Torsional, and Extensional Behavior. *PLoS Comput. Biol.* **2009**, *5*, e1000389.
39. Shams, H.; Golji, J.; Mofrad, M. R. K. Molecular Trajectory of Alpha-Actinin Activation. *Biophys. J.* **2012**, *103*, 2050–2059.
40. Phillips, J. C.; Braun, R.; Wang, W.; Gumbart, J.; Tajkhorshid, E.; Villa, E.; Chipot, C.; Skeel, R. D.; Kalé, L.; Schulten, K. Scalable Molecular Dynamics with NAMD. *J. Comput. Chem.* **2005**, *26*, 1781–1802.
41. MacKerell, a D.; Banavali, N.; Foloppe, N. Development and Current Status of the CHARMM Force Field for Nucleic Acids. *Biopolymers* **2001**, *56*, 257–265.
42. Nosé, S. A Unified Formulation of the Constant Temperature Molecular Dynamics Methods. *J. Chem. Phys.* **1984**, *81*, 511–519.
43. Humphrey, W.; Dalke, A.; Schulten, K. VMD-Visual Molecular Dynamics. *J. Mol. Graphics* **1996**, *14*, 33–38.